Queen's University Belfast

Correlation Between the Electrical and Optical Properties of an Atmospheric Pressure Plasma During Siloxane Coating Deposition

Twomey, B., Nindrayog, A., Niemi, K., Graham, B., & Dowling, D. P. (2011). Correlation Between the Electrical and Optical Properties of an Atmospheric Pressure Plasma During Siloxane Coating Deposition. Plasma Chemistry and Plasma Processing, 31(1), 139-156. DOI: 10.1007/s11090-010-9266-z

Published in:
Plasma Chemistry and Plasma Processing

Queen's University Belfast - Research Portal:
Link to publication record in Queen's University Belfast Research Portal

General rights
Copyright for the publications made accessible via the Queen's University Belfast Research Portal is retained by the author(s) and / or other copyright owners and it is a condition of accessing these publications that users recognise and abide by the legal requirements associated with these rights.

Take down policy
The Research Portal is Queen's institutional repository that provides access to Queen's research output. Every effort has been made to ensure that content in the Research Portal does not infringe any person's rights, or applicable UK laws. If you discover content in the Research Portal that you believe breaches copyright or violates any law, please contact openaccess@qub.ac.uk.

Download date:15. Feb. 2017

Correlation Between the Electrical and Optical Properties of an Atmospheric Pressure Plasma During Siloxane Coating Deposition

Plasma Chemistry and Plasma Processing

ISSN 0272-4324
Volume 31
Number 1

Plasma Chem Plasma Process
(2010) 31:139-156
DOI 10.1007/s11090-010-9266-z

Volume 31, Number 1
February 2011

31(1) 1–250 (2011)
ISSN 0272-4324

Plasma Chemistry and Plasma Processing

Available online
www.springerlink.com

Your article is protected by copyright and all rights are held exclusively by Springer Science+Business Media, LLC. This e-offprint is for personal use only and shall not be self-archived in electronic repositories. If you wish to self-archive your work, please use the accepted author's version for posting to your own website or your institution's repository. You may further deposit the accepted author's version on a funder's repository at a funder's request, provided it is not made publicly available until 12 months after publication.

Springer

Author's personal copy

Plasma Chem Plasma Process (2011) 31:139–156
DOI 10.1007/s11090-010-9266-z

ORIGINAL PAPER

Correlation Between the Electrical and Optical Properties of an Atmospheric Pressure Plasma During Siloxane Coating Deposition

B. Twomey · A. Nindrayog · K. Niemi · W. G. Graham · D. P. Dowling

Received: 13 January 2010 / Accepted: 18 October 2010 / Published online: 14 November 2010
© Springer Science+Business Media, LLC 2010

Abstract The effect of varying process parameters on atmospheric plasma characteristics and properties of nanometre thick siloxane coatings is investigated in a reel-to-reel deposition process. Varying plasma operation modes were observed with increasing applied power for helium and helium/oxygen plasmas. The electrical and optical behaviour of the dielectric barrier discharge were determined from current/voltage, emission spectroscopy and time resolved light emission measurements. As applied power increased, multiple discharge events occurred, producing a uniform multi-peak pseudoglow discharge, resulting in an increase in the discharge gas temperature. The effects of different operating modes on coating oxidation and growth rates were examined by injecting hexamethyldisiloxane liquid precursor into the chamber under varying operating conditions. A quenching effect on the plasma was observed, causing a decrease in plasma input power and emission intensity. Siloxane coatings deposited in helium plasmas had a higher organic component and higher growth rates than those deposited in helium/oxygen plasmas.

Keywords Atmospheric pressure plasma · Plasma diagnostics · Aerosol precursor · Thin films

Introduction

Atmospheric plasmas are increasingly used for the processing of materials in the packaging [1], biomedical [2], composite materials [3] and microelectronic industries [4]. With increased usage, the ability to characterise atmospheric pressure plasmas has become increasingly important. Plasma diagnostics typically incorporate extensive optical and

B. Twomey · D. P. Dowling (✉)
Surface Engineering Group, School of Electrical, Electronic and Mechanical Engineering, UCD, Belfield, Dublin 4, Ireland
e-mail: denis.dowling@ucd.ie

A. Nindrayog · K. Niemi · W. G. Graham
Centre of Plasma Physics, School of Mathematics and Physics, Queen's University, Belfast BT7 1NN, UK

Author's personal copy

electrical analysis techniques [5]. These include fast intensified charge coupled detector (ICCD) imaging [6–8] and the use of photomultiplier tubes [9, 10] to resolve time varying discharge events, optical emission spectroscopy (OES) [11, 12] and current and voltage waveform analysis [8, 13]. In recent years, coating technology has expanded to encompass coating deposition using atmospheric pressure plasma techniques. The introduction of a liquid precursor is typically carried out in the form of an aerosol via direct injection [14, 15] or as a gas via a bubbler system [16, 17]. Extensive analysis of coatings deposited in DBD systems has also enabled a detailed understanding of the precursor polymerisation, dissociation and deposition [18–21].

With the commercial exploitation of this technology it is increasingly important to understand the relationship between the atmospheric pressure plasma parameters and the properties of the deposited coatings. The objective of this study is to couple electrical and optical plasma characterisation with active coating deposition in a reel-to-reel atmospheric pressure plasma deposition system. Both He and He/O_2 environments are compared as the addition of O_2 has been shown to increase coating oxidation and density [20, 21]. Here the liquid precursor hexamethyldisiloxane (HMDSO) was nebulised into the plasma with the helium feed gas. By systematically altering the plasma deposition parameters, the physical and chemical properties of the resulting siloxane coatings are altered. The effect of incrementally changing liquid precursor flow rate and applied power was correlated with the plasma parameters (current, voltage and frequency and OES) as well as the physical and chemical properties of the siloxane coatings.

Experimental Work

Atmospheric Pressure Plasma Treatment

The coatings were deposited using the Dow Corning® SE-1100 Labline™ atmospheric pressure plasma system [18]. It comprises 2 vertical parallel-plate plasma chambers arranged in conjunction with a dedicated polymer film handling system. The electrode gap width is set at 5 mm. The 300 × 300 mm electrodes consist of a conductive liquid contained in a transparent dielectric housing. This enables the observation of discharge events across the entire electrode. Powers of up to 2,000 W can be applied to the two electrodes using a Vetaphone ac power supply (frequency c. 20 kHz). The power supply has a frequency agile impedance matching circuit, rather than altering inductor and capacitor elements. Circuit resonance is maintained using a pick-up coil on the transformer secondary winding, which sends the load voltage and current magnitude and phase to the matching circuit. Here the supply frequency is adjusted to ensure that the real component of the two complex impedances are of the same value and the imaginary component of the impedances is of the same but of opposite sign [22]. Manual rotameter valves are used to control gas flows. He and O_2 (when used) gas flow rates were maintained at 10 and 0.1 l/min, respectively. A syringe pump was used to supply the liquid precursor to 2 nebulisers (Burgener HP Ari Mist) positioned at the top of the plasma deposition chamber. The HMDSO siloxane precursor was sourced from Sigma–Aldrich with a purity of at least $\geq$98%. Polyethylene teraphthalate (PET) film of width 10 and 50 μm in thickness, available from AB Supplies Ltd (UK), was passed through the electrodes using the integrated polymer film handling system. The HMDSO was continuously nebulised into the plasma zone as the PET film was passed through the chamber at a speed of 1.5 m/min resulting in a residence/deposition time of 25 s per pass.

Author's personal copy

Current and voltage values are measured using a Pearson 6585 (1 A: 1 V) fast current monitor and a North Star PVM-5 (1 kV: 1 V) high voltage probe. These measurements are made at the output of the power supply and recorded with a Tektronix TDS2024 oscilloscope. For optical emission spectroscopy (OES) light from the discharge was collected through lenses mounted vertically above the discharge and carried to both Ocean Optics USB4000 UV/VIS and HR4000 spectrographs via a quartz fibre optic cables. The spectral range and resolution of the spectrographs are 200–880 and 0.2 nm full width half-maximum (FWHM) and 295–395 and 0.09 nm FWHM, respectively. The temporally resolved total emission was measured using a photomultiplier tube (PMT) (RCA 931A) with a rise time of 1 ns and 1 mm^2 circular entrance aperture. This viewed the discharge through the transparent face of one of the electrodes, which limited the spectral range to $\approx$400–800 nm. Spatially resolved images of the light emission from the discharge were obtained using a Sony Cyber-Shot C70 digital camera at constant exposure times/levels. A light intensity map was then generated from greyscale images using the Matlab 7 'surf' function.

Coating Characterisation

It has been demonstrated previously that surface energy measurements provide an indication of surface chemistry (level of oxidation) and precursor plasma polymerization [18, 23]. The surface energy was determined according to the sessile drop technique using an OCA 20 video capture apparatus from Dataphysics Instruments. Drop volumes of 1.5 µl of the following liquids were used to determine surface energy according to the OWRK method [24]: deionised water, diiodomethane and ethylene glycol. In each measurement, three drops were deposited over the width of the sample and their contact angle was measured after settling on the surface for 10 s. The coating surface energy was calculated from the average contact angle value measured 1 week after deposition for each of the probe liquids. This was done to eliminate any surface energy changes immediately after plasma treatment and hydrophobic recovery in the time period after deposition [25]. Coating morphology and surface roughness were examined using a Wyko NT1100 optical profilometer operating in phase shift interferometry (PSI) mode. The average surface roughness value was obtained for 10 measurements (Average roughness—R_a and Root Mean Square roughness—R_q). Coating thickness was measured using a Woollam M2000 variable wavelength spectroscopic ellipsometer. Fourier transform infrared spectroscopy (FTIR) measurements were carried out using a Bruker Vertex-70 system equipped with a DTGS (Deuterated Triglycine Sulfate) with a KBr beam splitter. The sample chamber was purged by N_2 gas before the scans were obtained. Spectra were collected in the range of 800–4,000 cm^{-1} using a spectral resolution of 4 cm^{-1}. The transmission spectra for siloxane coated NaCl disks were obtained by the overlay of 128 scans to increase signal to noise ratio. The NaCl IR cards were obtained from Apollo Scientific Ltd and had a 15 mm aperture. NaCl substrates were used to minimise substrate interference during the measurement of nanometre thick SiO_x coatings. The IR cards were mounted on the PET film during deposition using double sided tape. X-ray photoelectron spectroscopy (XPS) was performed using a Kratos Analytical Axis Ultra photoelectron spectrometer. The instrument is equipped with a spherical mirror analyser (165 mm mean radius HSA), an integral automatic charge neutraliser and a magnetic lens. A monochromated aluminium (Al Kα) X-ray source was used to record spectra at normal emission. All samples were stored at standard temperature and pressure before analysis.

Author's personal copy

Results and Discussion

The experimental results are divided into two sections. Firstly, the study of the effect of systematically altering applied power (500–2,000 W) to the He and He/O_2 atmospheric plasmas on current, voltage and emission spectra and gas temperature. Secondly, the liquid HMDSO precursor was nebulised into the plasma at flow rates in the range 12.5–50 μl/min. The effect of both precursor flow rate and applied power was examined both with respect to plasma parameters and the properties of the deposited siloxane coatings.

Discharge Dependence on Applied Power

Time Resolved Electrical and Emission Behaviour

In this study the effect of increasing applied power on the He and He/O_2 electrical (current/voltage waveform) and optical (PMT and OES) plasma properties are examined. The relationship between the power supply operating frequency, plasma input power W and the applied power as indicated on the power supply meter was explored. The plasma input power was calculated from Eq. 1 using the measured current and voltage waveforms [8]:

$$W = F \int_{t}^{t+T} I(t)V(t)dt \tag{1}$$

where F is frequency, $T = 1/F$ (period), V is voltage and I is current.

The values of the input power, rms voltage and operating frequency at a selection of applied powers are listed in Table 1 and discussed in detail elsewhere [26–28]. The efficiency of the system (calculated input power/applied power) increases with applied power from $\sim$20 to 45%. In He plasmas the frequency change is abrupt and occurs between 900 and 1,000 W, while in He/O_2 plasmas this change occurs gradually between 1,300 and 1,600 W.

It has been previously reported [9, 29] that both the frequency of operation and maximum applied voltage affect the number of discharges per half cycle of applied voltage. A discharge event is marked by a discrete electrical breakdown event initiating a pulse in the current signal and in the plasma emission detected in the PMT signal. At low applied powers, a single discharge event is observed in both the current and emission signals (Fig. 1). With increasing power the number of discharge events, per half cycle of the waveform, increased from 1 to 13 at 2,000 W for both He and He/O_2 discharges. Such

Table 1 Input power, RMS voltage and frequency for He and He/O_2 plasmas with increasing applied power

Applied power (W)	Helium			He/O_2		
	Input power (W)	V_{RMS} (kV)	Frequency (kHz)	Input power (W)	V_{RMS} (kV)	Frequency (kHz)
500	76	0.8	23.3	101	0.9	23.4
1,000	306	2.2	17.2	244	1.4	22.1
1,500	652	4.2	16.3	596	2.8	17.6
2,000	789	4.7	16.6	959	4.3	16.9

Author's personal copy

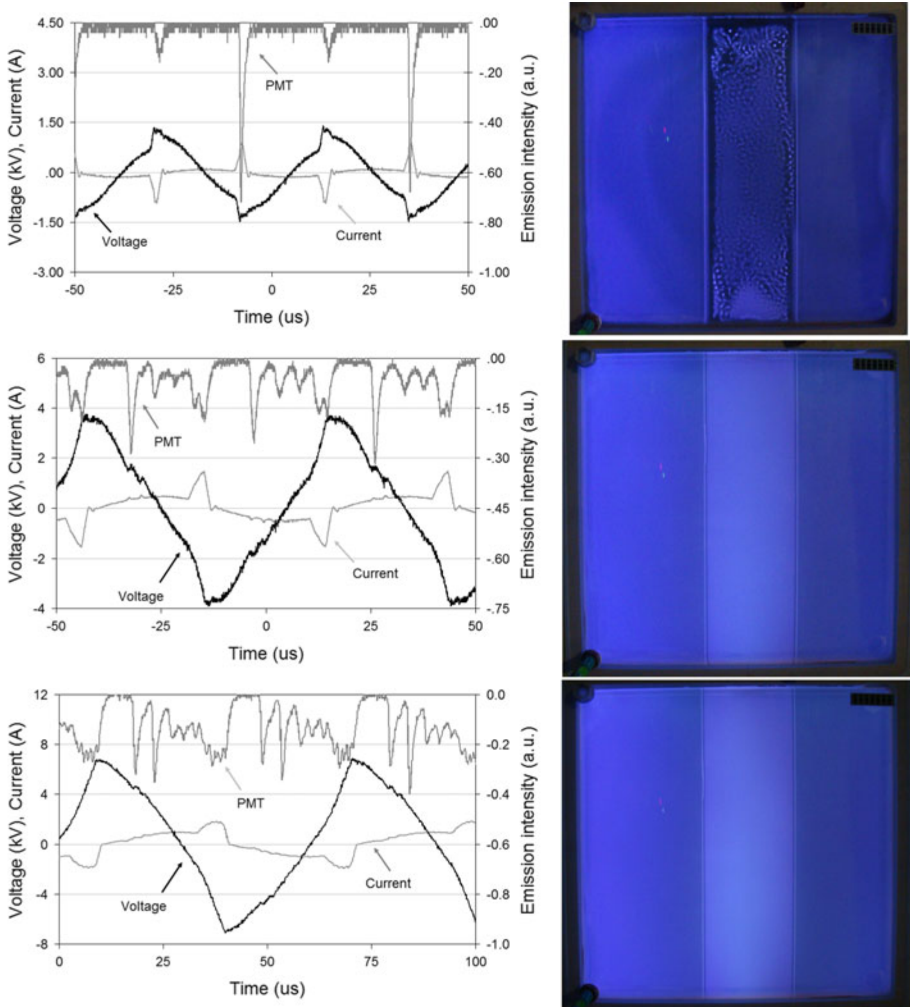

Fig. 1 Electrical discharge characteristics (*left*) and optical appearance (*right*) of a Helium discharge at increasing applied powers: 500 (*top*), 1,000 (*middle*) and 1,500 W (*bottom*). Note the presence of the 10 cm polymer web in the centre of the chamber

multiple discharges per half cycle, varying in number with both the frequency and amplitude of the applied voltage, have been previously reported in DBDs [18, 29–31]. These are generally explained as resulting from the maximum applied voltage exceeding the threshold breakdown voltage for the gap. Following a breakdown, a combination of residual charge, enhanced by the presence of N_2 impurity, and increasing applied voltage can generate a sufficiently high voltage across the gap that again exceeds the breakdown voltage of the gap resulting in a train of discharges that can therefore persist until close to the applied voltage maximum. However, it should be noted that the train of discharges observed in this system [27] are different from those previously reported [9, 32], in that the discharge current peaks do not sequentially decrease in magnitude. This may be because in

Author's personal copy

this larger area device, the discharge events are occurring at different locations on the electrode.

The FWHM of the emission peak for each discharge pulse in both He and He/O_2 plasmas is approximately 2 μs. In the more intense discharge events there is a steep rising onset of a few nanoseconds followed by a slower decay. The lower intensity discharges are more symmetric. This may indicate that different excitation processes are dominant in the two cases and suggests that temporal- or wavelength-dependent measurements are needed. In He/O_2 plasmas the behaviour is similar to that in He except the applied power required for the onset of multiple discharge events increases from approximately 800 to 1,200 W. This is because the applied voltages at the same applied powers are lower in the He/O_2 than in the He only plasma (Table 1). The discharge structure observed here has striking similarities to the atmospheric pressure glow discharge as described in [9, 11, 13, 29]. This is characterised by the formation of a large area of ionization near the cathode, the cathode fall, causing the electric field to be distorted resulting in a drop in the applied voltage.

Spatially Resolved Emission Behaviour

As the images in Figs. 1 and 2 illustrate for both He and He/O_2 discharges at lower applied powers, the plasma appears spatially homogeneous in the region outside of the polymer web. By contrast, in the area over the polymer film organized micro-discharge structures of the order of millimetres in diameter formed. Over the polymer film the micro-discharge structures are more diffuse with 'dark' regions with no discharge formation. In He/O_2 mixtures the areas both outside and over the film exhibit these micro-discharges. This feature of glow-type micro-discharges has been reported previously [10, 33, 34]. These discharge events were more common to He/O_2 plasmas and it has been suggested that this is due to the quenching effect of oxygen [35]. When oxygen is added to a He discharge then the primary ion becomes ${O_2}^+$, because of its significantly lower ionisation potential to that of He. The enhanced collisionality of the molecular gas means that the electron temperature drops and negative ions are formed, reducing the electron density. When combined with the fact that O_2 emission is predominantly in the UV region there is a decrease in the optical emission. As the applied power and hence peak voltage increases, the number of the micro-discharges increases and eventually coalesce to form a spatially homogeneous discharge, as also reported previously [33].

Optical Emission Spectroscopy

The enhanced plasma activity with increasing power, as indicated by the multi-peak behaviour of the discharge current, produces a visible increase in the overall light intensity emitted from the plasma. This is demonstrated using both the photomultiplier tube signal and the integrated area of the emission spectra. Examples of the latter are given in Fig. 3. The main emission lines between 300 and 435 nm are associated with the N_2 2nd positive $\left(C^3\Pi_u^+ \rightarrow B^3\Pi_g^+\right)$ bands and the ${N_2}^+$ 1st negative $\left(B^2\Sigma_u^+ \rightarrow X^2\Sigma_g^+\right)$ bands at 391 nm. The dominant He and O peaks are seen at 706.5 and 777.2 nm, respectively. The $N_2^+B^2\Sigma_g^+$ state is populated by near resonant Penning ionisation of nitrogen molecules by He metastables or dimers [36]. This makes the behaviour of this emission line a good indicator of helium metastable or dimer behaviour. Despite the sharp rise in voltage and shift in operating frequency with increasing applied power, shown in Fig. 1, the integrated light intensity and maximum voltage was found to vary linearly with input power.

Author's personal copy

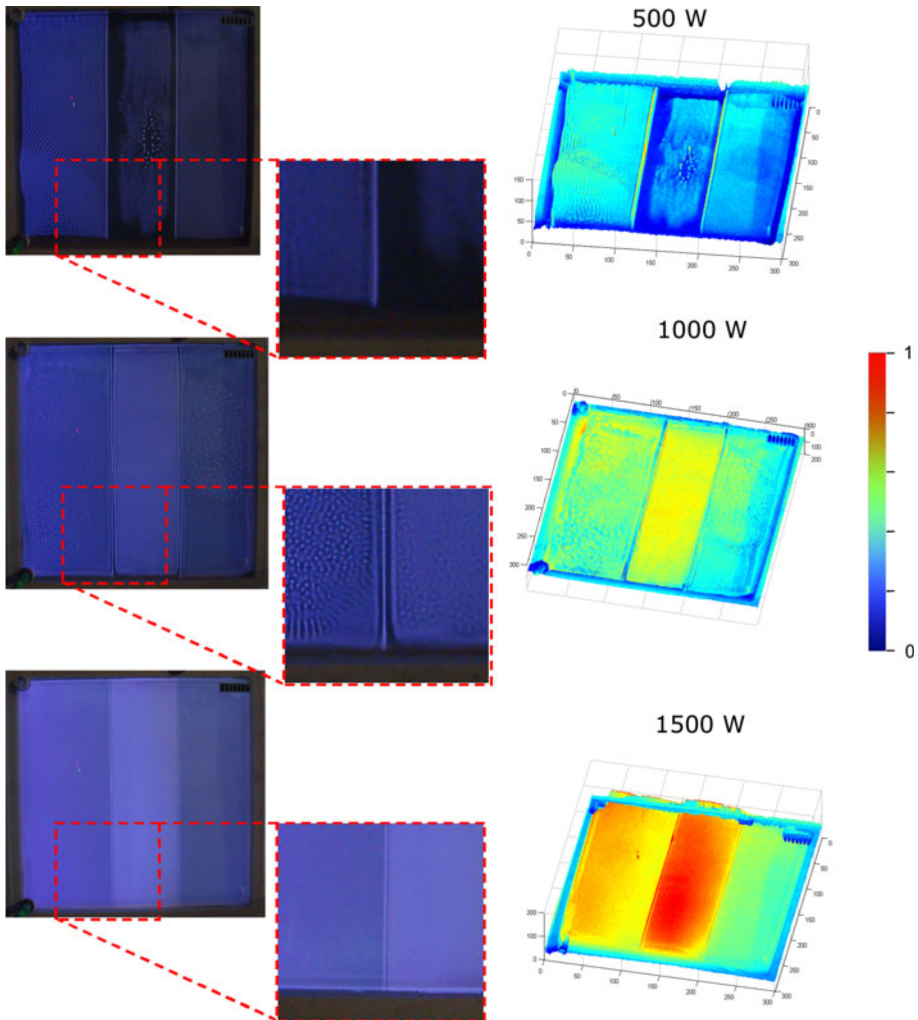

Fig. 2 Digital image of He/O_2 discharge (*left*) and light intensity map of greyscale images (*right*) at 500, 1,000 and 1,500 W applied power (0 *black*, 1 *white*). Note the presence of the 10 cm polymer web in the centre of the chamber

It was observed that all the main emission peaks (N_2, N_2^+, He and O) increased with a similar trend to that observed for the total emission intensity. In order to determine the effect of increasing voltage on these species, emission intensity ratios were examined. As shown in Fig. 4, in examining the N_2^+/N_2 intensity ratio for the dominant emission peaks, it was observed that in a He only plasma, the ratio increased as the applied voltage increased up to a value corresponding to an applied power of about 1,000 W. This indicates increasing He metastable and dimer production with applied power. Above this power, the ratio stabilises. The increasing value of this ratio indicates that the electron temperature is increasing up to about 900 W after which it remains approximately constant. This is probably due to plasma being present for an increasingly larger portion of the applied voltage half cycle.

Author's personal copy

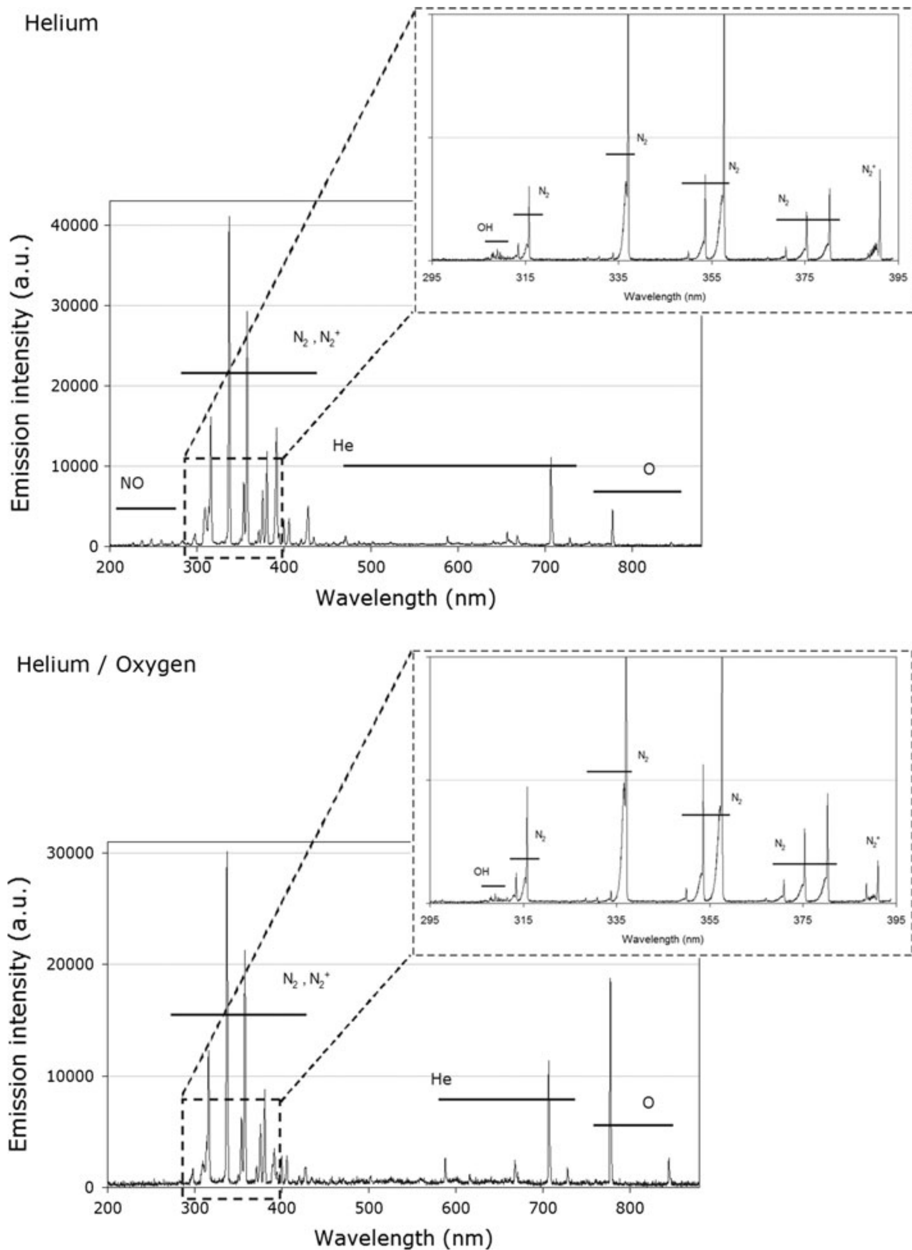

Fig. 3 Optical emission spectra from a He (*top*) and a He/O_2 (*bottom*) plasma operating at 2,000 W with high resolution OES (*insert*)

In He/O_2 discharges the amount of oxygen added (1%) is expected to exceed that of the residual N_2 from the atmosphere and as an impurity in the He gas. The addition of O_2 to a He plasma causes significant plasma quenching [19, 37] resulting in a different trend in the N_2^+/N_2 intensity ratio (Fig. 4). The additional inelastic electron collision processes with

Author's personal copy

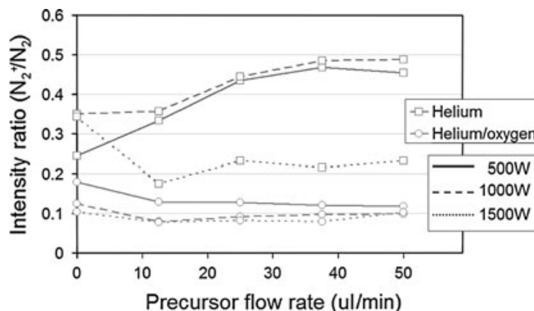

Fig. 4 Examining the effect of the addition, to both He only and He/O_2 plasmas, of HMDSO and its flow rate on) on the N_2^+/N_2 species ratio at various applied powers

the molecular oxygen will also reduce the electron temperature. Both processes will favour N_2 excitation over that of the N_2^+ band. The cumulative effect is seen in the decrease of the N_2^+/N_2 intensity ratio with increasing power in Fig. 4. The ratio is then essentially constant above an applied power close to the frequency transition point, for the same reasons as discussed for He above. It has been previously reported that in atmospheric pressure plasmas, O_2 molecules are dissociated via energy transfer from He metastables [5, 19]. The O (777.2)/N_2^+ ratio was observed to increase with increasing applied power, supporting this hypothesis. This is indicative of significant differences in the active species present between He and He/O_2 discharges despite similarities observed in the discharge characteristics at increased applied powers [27].

The addition of HMDSO to the plasma has an interesting effect on the line ratio. It is expected that this complex molecular gas will reduce the electron temperature. The relatively low ionisation potential of 9.6 eV [38] suggests that it will be readily ionized. When added to a He plasma operating in the low power (500 W) mode there is a rapid decrease in the ratio which implies significant quenching of the helium metastables. However, at higher powers where there is initially higher ionisation, this effect is reversed and an as yet unexplained increase in the ratio occurs. When added to a He/O_2 plasma the effect of the addition HMDSO molecules is less; however, a small flow of precursor causes a relative decrease in the ratio at all powers but there is little change beyond flow rates of 12.5 μl/min.

Determining Gas Temperature from Emission Spectroscopy

It is generally considered that the population distribution among rotational sublevels of molecular nitrogen is closely coupled to the translational energy distribution of the gas, and so the rotational temperature is close to the kinetic gas temperature [39]. Here, the rotational temperature T_{rot} was determined from the optical emission spectra of the persistent nitrogen gas impurities present in an open air atmospheric pressure system. The evaluation concentrates on the $v = 0 \rightarrow 2$ rotational band of the N_2 ($C^3\Pi_u^+ \rightarrow B^3\Pi_g^+$) second positive system, as shown in Fig. 5, since it has been found to be free from overlap with other spectral features and the small quantum numbers of the states means that their population distribution is likely to be closer to equilibrium leading to the most reproducible results. The results are obtained by numerically fitting a simulated spectrum to the measuring points. The simulation is based on spectral data [40] and line strengths [41] for the present transition from Hund's case b to intermediate coupling; Λ-doubling of the resulting 27 rotational branches is neglected. The Newton-Gauss algorithm is used for iterative least square (χ^2) minimization; rotational temperature, overall intensity, FWHM of the Gaussian apparatus function, a wavelength shift, and a background level are varied simultaneously.

Author's personal copy

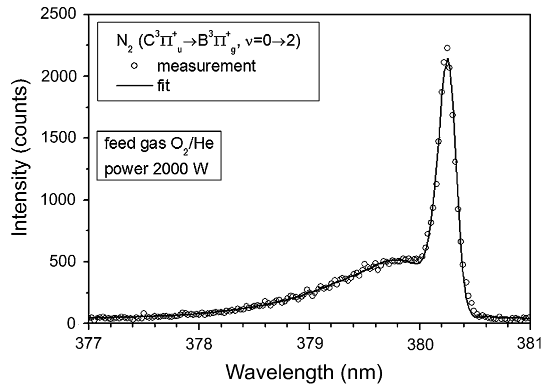

Fig. 5 Measured optical emission spectrum of N_2 ($C^3\Pi_u^+ \rightarrow B^3\Pi_g^+$, $v = 0 \rightarrow 2$), in this case for He/O_2. The *solid line* represents the 'best fit' simulated spectrum

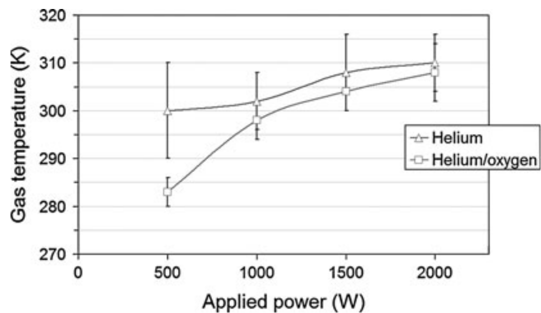

Fig. 6 Rotational temperature as a function of applied power for He and He/O_2 discharges

The calculated rotational temperature and hence gas temperature, even at the highest applied power in a He discharge, does not exceed 310 ± 20 K and shows little variation with applied power. The errors associated with T_{rot}, as shown in Fig. 6, are the statistical errors of the parameters determined from the covariance matrix for the converged solution. At the lowest powers the temperature in He/O_2 is just measurably lower than in He. As previously discussed, significant quenching is observed with the addition of O_2 and this appears to have an effect on gas temperature at lower applied powers. As the discharge becomes more uniform with increasing applied power, the gas temperature of the He and He/O_2 discharges converge, as observed with the electrical characteristics.

During normal operation of the system, the temperature of the water based electrodes is observed to increase by up to 30 K in the low frequency, higher power modes. Although there is a circulating air cooling system in use on the electrode faces, some hysteresis (up to 10 K) was observed for gas temperature measurements with increasing and decreasing applied powers. This issue became more apparent during the longer processing times required for coating deposition under static applied power conditions. Although the injection of the precursor into the discharge results in plasma quenching, and an associated reduction in the optical emission signal and input power, no significant temperature decrease was observed. In fact, a slight increase was observed (10 K) in regimes operating at lower frequencies and higher input powers. The increased chamber heating rate in these regimes resulted in an increase in the overall temperature of the operating environment. As a result the effect of precursor addition on gas temperature cannot be addressed accurately in the current system configuration.

Author's personal copy

Siloxane Coating Deposition in He and He/O_2 Plasmas

The effect of increasing applied power on the electrical and optical properties of both He and He/O_2 plasmas was examined in the previous section. The work presented in this section studies the effect of introducing a HMDSO precursor on the plasma properties. The effect of adding this precursor at a range of different flow rates is examined for applied powers of 500, 1,000 and 1,500 W. Although in the previous section, He and He/O_2 discharges at these applied powers were shown to be significantly different, these powers are chosen for comparative purposes. This study evaluates the effect of precursor addition on both the plasma parameters as well as the physical and chemical properties of the deposited coatings.

Influence of Siloxane Precursor Introduction on Plasma Parameters

Siloxane coatings were deposited onto PET and silicon wafer substrates mounted onto the polymer film. In order to build up coating layers, the polymer is passed a number of times through the deposition chamber. Each deposition was carried out over four passes through the chamber resulting in a total deposition-time of 100 s. The flow rate of the HMDSO precursor was systematically increased from 12.5 to 50 μl/min per nebuliser.

Examining the emission characteristics of the plasma with the addition of precursor, it was observed that increased precursor volume (up to 50 μl/min) resulted in significant drop (>45%) in emission intensity. This corresponded with a decrease in the plasma input power of up to 10% at a constant applied power (unless otherwise stated). With increasing precursor volume in the plasma, the main N_2, N_2^+ and O species at 337, 391 and 777 nm, respectively, were observed to decrease, while little or no decrease was observed for the He peak at 706.5 nm. The addition of precursor to both the He and He/O_2 discharges resulted in weak emission lines identified as the atomic hydrogen Balmer alpha line at 656.2 nm and the CO ($B^1\sum \rightarrow A^1\Pi$) transitions at 451.1, 483.5, 519.8 561.0, 608 and 662 nm, as illustrated in Fig. 7 [42, 43]. There was no significant increase in the absolute intensity of the CO or H emissions, with increasing precursor flow rate although this was observed with increasing applied power. This indicates that the input power is still being transferred to helium; however, with the addition of the precursor, the resulting free electrons and metastables are consumed by the precursor and not by the N_2 and O_2 present.

A significant exception to this observation was observed however, for coatings deposited near the power transition point at 1,000 W in a He plasma. When the precursor flow rate is introduced (0–50 μl/min) near this transition point [26], the matching system reverts back to a high frequency, low efficiency mode of operation [27]. Due to this shift in operating mode, the total emission intensity drops significantly. This is accompanied by a decrease of 30% in the plasma input power. This transition, as shown in Fig. 8, highlights the significant effect precursor addition can have on the plasma characteristics during operation. Increasing precursor flow rates result in a similar transition, although not as abrupt, for He/O_2 discharges at 1,500 W applied power.

Examination of Deposited Siloxane Coatings

It has been previously reported that the addition of a siloxane precursor into an atmospheric pressure plasma has a quenching effect on the plasma resulting in a decrease in the input power and emission intensity of the plasma [18]. This quenching effect increases as the precursor concentration increases due to consumption of He metastables in a similar way to

Author's personal copy

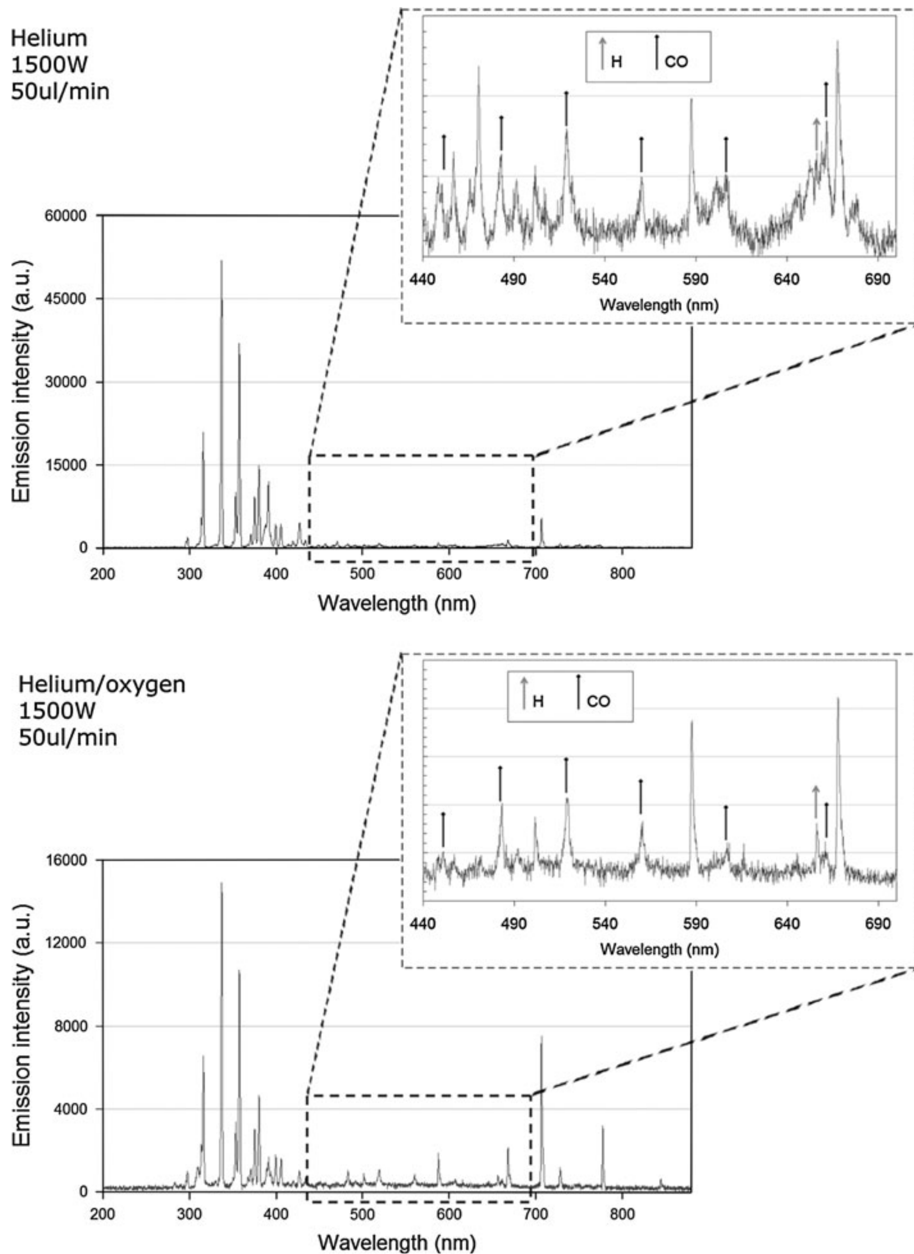

Fig. 7 Optical emission spectra from a He (*top*) and a He/O_2 (*bottom*) plasma operating at 1,500 W with a HMDSO precursor flow rate of 50 µl/min. Weak emission lines for CO and H observed between 440 and 700 nm (*insert*)

that of reported for oxygen [19]. The effect of increasing the flow rate of the HMDSO precursor from 12.5 to 50 µl/min on the properties of the deposited siloxane coatings was initially evaluated using surface energy measurements. As illustrated in Fig. 9, as the

Author's personal copy

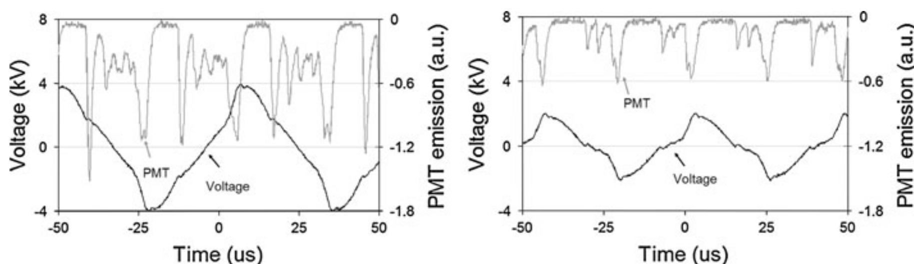

Fig. 8 Effect of precursor addition on the plasma characteristics: He plasma at 1,000 W, *left* 0 μl/min, *right* 50 μl/min

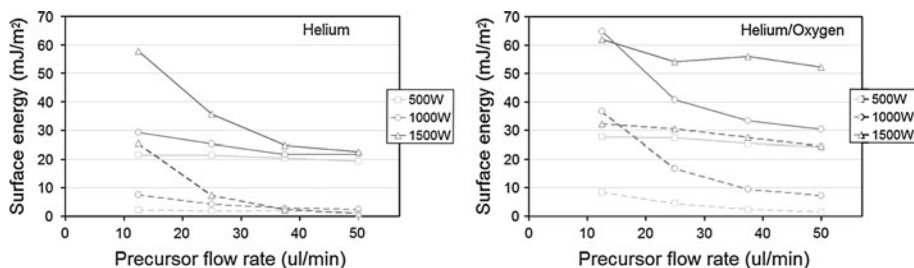

Fig. 9 Effect of increasing precursor flow rate on coating surface energy (*solid line*) for coatings deposited in a He (*left*) and a He/O_2 (*right*) plasma at: 500, 1,000 and 1,500 W: Polar component (*broken line*)

precursor flow rate increases in both the He and He/O_2 plasmas there is a decrease in surface energy and in particular, the polar component which was found to decrease to almost zero. Due to the decreased polarity of the Si–C bond over the Si–O bond, a decrease polar component indicates a decrease in the oxygen content of the deposited coatings and as a result, a decrease in coating oxidation [18, 23].

In order to investigate this further, FTIR analysis was carried out on a select number of coatings: 12.5 and 37.5 μl/min for He and He/O_2 at 1,500 and 1,000 W, respectively. XPS was also carried out on the He/O_2 deposited coatings. These flow rates were chosen as they exhibit a marked difference in surface energy values. Despite the differences in applied powers, He deposited coatings at 1,500 W exhibited similar surface energy values to the He/O_2 coatings deposited at 1,000 W. The FTIR spectra of the measured coatings (Fig. 10) were normalised to the $\approx$1,060 cm^{-1} peak for comparative purposes as differences in coating thickness will result in different peak intensity values [44]. It can be seen in Fig. 10 that for coatings deposited in He and He/O_2, the dominant Si–CH_3 peaks of the HMDSO monomer at 840, 1,260 and 2,960 cm^{-1} are increasingly retained with increasing precursor flow rate. This is in good agreement with the surface energy results.

Coatings deposited at 12.5 μl/min in He/O_2 exhibit a sharper peak at 1,060 cm^{-1} and no observable CH_3 functionality. Si–OH characteristics were observed in both coatings at 930 cm^{-1} and a broad peak at 3,400 cm^{-1}. These peaks increased with increasing precursor flow rates. As the spectra have been normalised, the full width at half maximum (FWHM) of the peak between 980 and 1,240 cm^{-1} can be easily compared. An increase in the FWHM indicates decreased coating homogeneity [45] and a broad shoulder may be attributed to coating porosity [43].

Author's personal copy

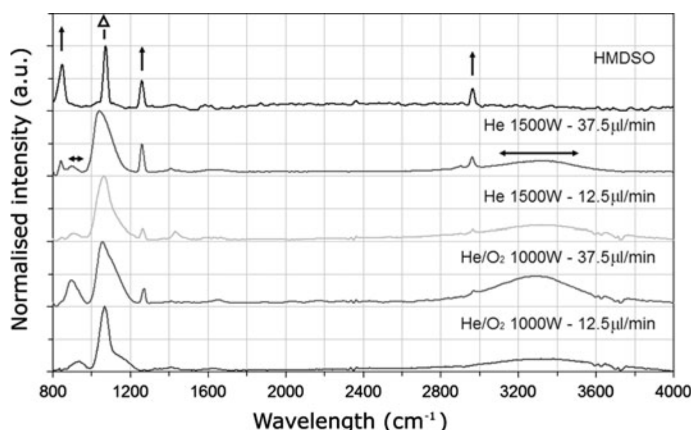

Fig. 10 FTIR spectra of HMDSO monomer and He and He/O_2 deposited coatings at increasing precursor flow rates. Peak reference: ↔ for OH, ↑ for CH_3 and Δ for Si–O–Si

Table 2 Change in coating elemental composition with increasing precursor flow rates for HMDSO coatings deposited in a He/O_2 plasma at 1,000 W

Precursor flow rate (µl/min)	Surface energy (mJ/m^2)	Elemental composition (%)			Siloxy chemistry (%)			
		O	C	Si	M	D	T	Q
12.5	64.8	59	9	32	0	6	15	79
37.5	33.4	29	46	26	9	58	33	0

XPS analysis was carried out to evaluate the effect of increasing HMDSO precursor flow rates from 12.5 to 37.5 µl/min on siloxy chemistry. The coatings were deposited in a He/O_2 plasma at an applied power of 1,000 W. As shown for the elemental composition analysis given in Table 2, with increased precursor flow rate the oxygen content of the coating decreases with a corresponding increase in carbon concentration. This correlates well with the corresponding decrease in surface energy values. The decrease in surface energy is further reflected in a change in the siloxy chemistry of the coatings with the retention of methyl groups and reduced crosslinking and oxidation at higher precursor flow rates. Curve fitting of the silicon (Si 2p) core level was carried out to provide the siloxy chemistry of the coating. The process is described in detail elsewhere [46]. The simplified siloxy chemistry notation used to represent the number of oxygen atoms attached to the silicon is as follows [46]: M [$(CH_3)_3SiO_{1/2}$], D [$(CH_3)_2SiO_{2/2}$], T [$(CH_3)SiO_{3/2}$] and Q [$SiO_{4/2}$]. As summarised in Table 2, the dominant chemistry for coatings deposited at 37.5 µl/min is D- and T-type (91%), indicating limited polymerisation of the M-type HMDSO precursor bond. For coatings deposited at 12.5 µl/min, the dominant chemistry is T- and Q-type (94%). As a result of O_2 addition, coatings deposited at lower precursor flow rates exhibit increased oxidation, homogeneity and a decreased organic fraction.

The effect of increasing the applied power with HMDSO precursor flow rate on coating growth rates was examined for both He and He/O_2 plasmas. The applied power was evaluated at 500, 1,000 and 1,500 W. As shown in Fig. 11, as both the HMDSO precursor flow rate and applied power is increased there is a corresponding increase in coating

Author's personal copy

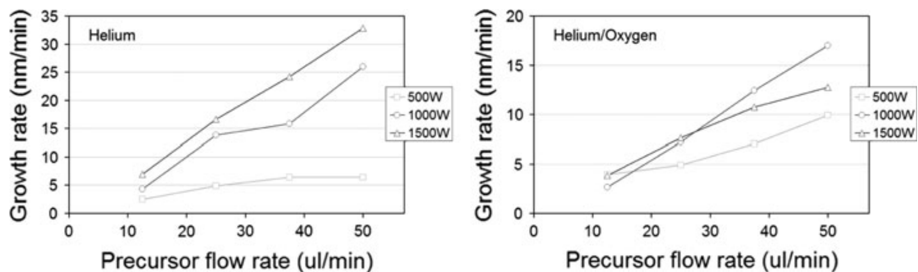

Fig. 11 Effect of increasing precursor flow on coating growth rate at varying powers applied to a He (*left*) and He/O_2 (*right*) plasma

Table 3 Flux and oxidation efficiency of coatings deposited at 25 µl/min in He and He/O_2 discharges at 500, 1,000 and 1,500 W applied power

Applied power (W)	Flux efficiency (%)		Coating oxidation rate (%)	
	He	He/O_2	He	He/O_2
500	4.4	4.4	4.2	16.0
1,000	12.4	6.5	11.7	42.4
1,500	15.0	6.8	32.4	68.6

growth rate. The thickness of coatings deposited in He plasmas were however significantly greater than He/O_2 plasmas for equivalent applied powers. These latter coatings also exhibited higher surface energies (>55 mJ/m^2) compared with the coatings deposited using the He only plasma (<30 mJ/m^2). It has been shown previously that higher surface energy values can be correlated with increased coating oxidation indicating increased coating density [18], as indicated by the FWHM observed with FTIR. Increased coating oxidation will result in lower coating growth rates through densification. The significant reduction in active species in the plasma due the addition of O_2 will also affect coating growth rates and coating chemistry.

Based on coating growth rates, the flux efficiency (precursor volume/coating volume) was calculated for coatings deposited at 25 µl/min for He and He/O_2 discharges. This flow rate was chosen as there is a step change in surface energy values for coatings deposited at varying level of applied power. As shown in Table 3, the flux efficiency increases with increasing applied powers: from 4 to 15% for He and 4 to 7% for He/O_2. The decreased flux efficiency for coatings deposited in He/O_2 discharges is likely the result of two factors. Firstly, the decreased input power for He/O_2 discharges for equivalent applied powers compared to He discharges. Secondly, the increased oxidation of coating deposited in He/O_2 discharges will result in a denser coatings that exhibit lower coating growth rates [18]. Based on the lowest surface energy value achieved (HMDSO at 50 µl/min in He discharge at 500 W applied power—19.3 mJ/m^2) and a maximum surface energy value of 70 mJ/m^2 for a highly oxidised HMDSO coating (90% Q-type chemistry) [18], the coating oxidation rate was observed to be significantly higher for coatings deposited in He/O_2 then He discharges (Table 3). Therefore, despite the lower input powers observed for He/O_2 discharges when compared to He discharges at equivalent applied powers, the presence of reactive atomic oxygen species is more important when increased levels of coating oxidation are desired.

Author's personal copy

Coating Morphology

The effect of increasing applied power on coating morphology was examined using optical profilometry. It was observed that surface roughness (R_a and R_q) increased with both increasing applied power and precursor flow rate (Table 4). The increasing surface roughness was a result of increasing number of particulates deposited on the coating. Particulate formation is commonly associated with gas phase reaction [14]. As discussed previously, the addition of the precursor quenches the main emission lines of N_2, N_2^+ and O i.e. the precursor consumes the active species that would otherwise increase the intensity of these lines.

With increased precursor flow rates, there is a reduction in active species present in the plasma resulting in incomplete polymerisation and hence, the formation of non-stoichiometric particles (Fig. 12). It has previously been reported that larger, non-stoichiometric particles are generally formed at high precursor flow rates while nano-scale stoichiometric particles are formed at lower flow rates [47]. With increasing applied power, there are increased concentrations of active species in the plasma, as indicated by both multi-peak behaviour and increased emission intensity. This is expected to result in an increased level of gas phase reactions. The addition of oxygen was also found to increase the number of surface particulates. This is due to the high reactivity of excited oxygen species [19] resulting in oxidative gas phase reaction and the formation of Si-$(OH)_4$ type particles, observed by FTIR in Fig. 10. As a result, coatings deposited in He/O_2 generally exhibited higher surface roughness values than He deposited coatings. Despite differences in coating growth rates between He and He/O_2, the same particulate formation trends were observed in both plasmas i.e. increased power leads to increased gas phase reaction and increased precursor flow rates leads to the formation of non-stoichiometric particles. As a result,

Table 4 Effect of increasing applied power and precursor flow rate on the surface roughness of coatings deposited on silicon wafer substrates (50 × 50 µm area)

Applied power (W)	Flow rate (µl/min)	He		He/O_2	
		12.5	50	12.5	50
500	R_a (nm)	0.37	0.34	0.38	0.44
	R_q (nm)	0.55	0.51	0.57	0.98
1,000	R_a (nm)	0.38	0.75	0.36	0.69
	R_q (nm)	0.68	1.34	0.45	1.40
1,500	R_a (nm)	0.52	0.91	0.57	1.10
	R_q (nm)	0.81	1.27	0.93	1.83

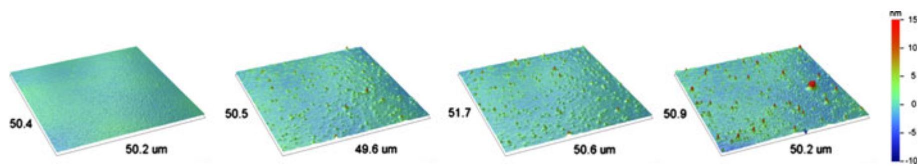

Fig. 12 Surface morphology of coatings deposited in a He/O_2 discharge at 1,000 W applied power (50 × 50 µm area). HMDSO precursor flow rate *left* to *right* 12.5, 25, 37.5 and 50 µl/min

Author's personal copy

coating surface roughness (R_a and R_q) was observed to increase with the increase in applied power and precursor flow rates (Table 4).

Conclusions

In this study the effect of varying gas composition, applied power, HMDSO precursor flow rate on both plasma parameters and deposited siloxane coating properties has been correlated. At low applied plasma powers, an inhomogeneous discharge was observed for both He and He/O_2. As the applied powers were increased the micro-discharges increased in number and eventually coalesced. This point corresponded with a frequency shift induced in the power supply in conjunction with an increase in peak voltage resulting in the formation of a 'pseudoglow', multi-peak discharge. The discharge peaks were observed to increase with increasing voltage, rather than frequency. The increase in discharge events resulted in an increase in active species in the plasma, as measured using OES. The total plasma emission was observed to linearly increase with increasing voltage, showing a strong correlation between the optical and electrical plasma characteristics. A method to measure the plasma gas temperature from the rotational band emission of the N_2 s positive system has been applied. Lower temperatures, of about 20 K, were observed with the addition of O_2 to the He discharge although as the applied power increased and the electrical characteristics started to normalise, the temperature values also started to merge. Fitting the 0-2 band was found to exhibit the lowest measurement error. At higher applied powers, the issue of chamber heating becomes more of an issue with an increased rate of heating observed at higher powers. Further work needs to be carried out to examine the effect of an increased environmental temperature on coating properties.

With the addition of HMDSO precursor into the discharge, plasma quenching was observed due to the consumption of free electrons. The rate of chamber heating dictated that no resulting drop in gas temperature was observed. The coating oxidation rate was observed to decrease with increasing precursor flow rate. The addition of 1% O_2 resulted in increased oxidation and lower coating growth rates compared with coatings deposited in a pure He discharge. As indicated by the flux and coating efficiency, coatings deposited in a He discharge will result in increased coating thickness and increased functionality retention. The addition of O_2 results in increased crosslinking and coating oxidation, although the potential coating growth rate is limited by comparison to He deposited coatings. Although increasing applied power will result in increased coating growth rates and oxidation for both He and He/O_2 deposited coatings, higher concentrations of particulates are observed as a result of increased gas phase reactions. The deposition of highly oxidised or polymeric coatings can be achieved by varying the process parameters, but it has been shown that each variation will have a resultant affect on the plasma and coating properties.

Acknowledgments This work is partially supported by the Science Foundation Ireland Precision CLUSTER, Grant 08/SRC11411.

References

1. Chatham H (1996) Surface Coatings Technol 78:1
2. Hettlich HJ, Otterbach F, Mittermayer C, Kaufmann R, Klee D (1991) Biomaterials 12:521
3. Mohan J, Murphy N, Ivankovic A, Dowling D (2008) 17th European conference on fracture. Brno, Czech Republic, p 306

Author's personal copy

4. Schmid U, Seidel H (2006) Sens Actuat A Phys 194:130–131
5. Yokoyama T, Kogoma M, Moriwaki T, Okazaki S (1990) J Phys D Appl Phys 23:1125
6. Roth JR, Jozef R, Xin D, Daniel MS (2005) J Phys D Appl Phys 38:555
7. Starostin SA, ElSabbagh MAM, Aldea E, de Vries H, Creatore M, van de Sanden MCM (2008) IEEE Trans Plasma Sci 36:968
8. Massines F, Gouda G (1998) J Phys D Appl Phys 31:3411
9. Radu I, Bartnikas R, Wertheimer MR (2003) IEEE Trans Plasma Sci 31:1363
10. Radu I, Bartnikas R, Czeremuszkin G, Wertheimer MR (2003) IEEE Trans Plasma Sci 31:411
11. Nersisyan G, Graham WG (2004) Plasma Sources Sci Technol 13:582
12. Arkhipenko VI, Kirillov AA, Simonchik LV, Zgirouski SM (2005) Plasma Sources Sci Technol 14:757
13. Massines F, Gherardi N, Naude N, Segur P (2005) Plasma Phys Control Fusion 47:B577
14. Ramamoorthy A, Rahman M, Mooney DA, Don MacElroy JM, Dowling DP (2008) Surface Coatings Technol 202:4130
15. O'Neill L, O'Hare LA, Leadley SR, Goodwin AJ (2005) Chem Vapor Deposit 11:477
16. Zhu X, Arefi-Khonsari F, Petit-Etienne C, Tatoulian M (2005) Plasma Process Polym 2:407
17. Vangeneugden D, Paulussen S, Goossens O, Rego R, Rose K (2005) Chem Vapor Deposit 11:491
18. Twomey B, Rahman M, Byrne G, Hynes A, O'Hare L-A, O'Neill L, Dowling D (2008) Plasma Process Polym 5:737
19. Sawada Y, Ogawa S, Kogoma M (1995) J Phys D Appl Phys 28:1661
20. Starostine S, Aldea E, de Vries H, Creatore M, van de Sanden MCM (2007) Plasma Process Polym 4:S440
21. Sonnenfeld A, Tun TM, Zajíčková L, Kozlov KV, Wagner HE, Behnke JF, Hippler R (2001) Plasmas Polym 6:237
22. Ellingboe AR, Law VJ, Soberon F, Garcia F, Graham W (2005) Electron Lett 41:525
23. Twomey B, Dowling D, Byrne G, O'Neill L, O'Hare L-A (2007) Plasma Processes Polym 4:S450
24. Owens DK, Wendt RC (1969) J Appl Polym Sci 13:1741
25. Hillborg H, Gedde UW (1998) Polymer 39:1991
26. Tynan J, Law VJ, Twomey B, Hynes AM, Daniels S, Byrne G, Dowling DP (2009) Meas Sci Technol 20:115703
27. Twomey B, Dowling DP, Byrne G, Graham WG, Schaper LF, Della Croce D, Hynes A, O'Neill L (2009) IEEE Trans Plasma Sci 37:961
28. Law VJ, O'Connor N, Daniels S, Twomey B, Tynan J, Dowling DP, Byrne G (2009) CHAOS 2008 international conference, Crete. World Scientific Publishing Company, Greece, p 204
29. Xu X, Ou Q, Zhong S, Shu X, Meng Y (2006) Plasma Sci Technol 8:303
30. Mangolini L, Orlov K, Kortshagen U, Heberlein J, Kogelschatz U (2002) Appl Phys Lett 80:1722
31. Golubovskii YB, Maiorov VA, Behnke J, Behnke JF (2003) J Phys D Appl Phys 36:39
32. Wang D, Wang Y, Liu C (2006) Thin Solid Films 506–507:384
33. Boyers DG, Tiller WA (1982) Appl Phys Lett 41:28
34. Kogelschatz U (2002) IEEE Trans Plasma Sci 30:1400
35. Yang S, Gupta MC (2004) Surf Coatings Technol 187:172
36. Pouvesle JM, Bouchoule A, Stevefelt J (1982) J Chem Phys 77:817
37. Yu QS, Yasuda HK (1998) Plasma Chem Plasma Process 18:461
38. Hess GG, Lampe FW, Sommer LH (1965) J Am Chem Soc 87:5327
39. Ricard A, Nouvellon C, Konstantinidis S, Dauchot JP, Wautelet M, Hecq M (2002) J Vacuum Sci Technol A Vacuum Surf Films 20:1488
40. Roux F, Michaud F, Vervloet M (1993) J Mol Spectrosc 158:270
41. Kovács I (1966) Astrophys J 145:634
42. Pearse RWB, Gaydon AG (1965) The identification of molecular spectra. Chapman & Hall, London
43. Goujon M, Belmonte T, Henrion G (2004) Surf Coatings Technol 756:188–189
44. Rochat N, Chabli A, Bertin F, Vergnaud C, Mur P, Petitdidier S, Beeson P (2003) Mater Sci Eng B 102:16
45. Tomozieu N (2006) Appl Surf Sci 253:376
46. O'Hare L-A, Hynes A, Alexander MR (2007) Surf Interface Anal 39:926
47. Hollenstein C, Howling AA, Courteille C, Magni D, Scholz SM, Kroesen GMW, Simons N, Zeeuw Wd, Schwarzenbach W (1998) J Phys D Appl Phys 31:74